Energy Equip. Sys./ Vol. 11/No. 2/June 2023/ 123-144

ENERGY EQUIPSYS

Energy Equipment and Systems
http://energyequipsys.ut.ac.ir
www.energyequipsys.com

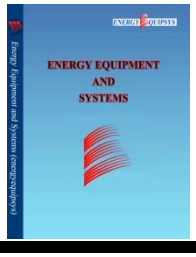

Transient simulation and 4E Analyses of a hybrid renewable energy system for an educational building

Authors

Sadegh Nikbakht Naserabad[a]
Roohollah Rafee[a*]
Seyfolah Saedodin[a]
Pouria Ahmadi[b]

[a] Faculty of Mechanical Engineering, Semnan University, 35131-19111 Semnan, Iran

[b] School of Mechanical Engineering, College of Engineering, University of Tehran, 11155-4563 Tehran, Iran

Article history:

Received : 5 October 2021
Accepted : 7 December 2021

ABSTRACT

In this research, an integrated fossil-solar energy system has been designed, modeled, and optimized to supply the required loads of a six-story educational building in Tehran. The three heating, cooling, and electrical loads of the building are extracted in an hourly dynamic pattern for one year. System modeling was performed using a developed code in MATLAB software, and the genetic algorithm was used for two and three objective optimizations. The results show that with the two objectives of exergy efficiency and pollution, 68 rows of PVT panels and a solar collector with an area of 6.25m² should be used. In this case, the maximum use of solar energy to supply 1945.9MWh heat and 484.5MWh electricity occurred during a year. Also, the highest amount of purchased electricity from the grid is 501.9MWh when the exergy efficiency and cost rate are considered as objective functions. In the three-objective optimization, the best system has an exergy efficiency of 50.21%. The CO_2 emission and total cost rate are 7.1$/h and 301g/kWh, respectively. In this case, about 583.06 kWh of the heating load is supplied annually by 20 rows of PVT and a solar collector which has an area of 5.27m². Photovoltaic panels generate 144.1MWh of the system's required electricity. The electricity sold to the grid in this scenario is 55.05MWh. Also, the system has purchased 204.2MWh of electricity from the grid annually. This means that the system should buy electricity from the grid most of the time each year.

Keywords: (4E) Analysis, Optimization, Building, Renewable Energy, Dynamic Simulation.

1. Introduction

Due to the growing importance of energy and environmental issues in the world and Iran, energy optimization strategies and the use of renewable energy sources have been considered by researchers. More than a third of fossil fuel energy is consumed in buildings. In recent years, peak consumption has always been related to household consumption [1]. Therefore, building energy optimization and the use of clean energy sources have become particularly important in today's world. The importance of optimizing building structure can be seen in the research by Sajjadi et al. [2]. This paper evaluates the use of electrochromic and thermochromic windows in building energy consumption. The results of this analysis show that the use of thermochromic windows has reduced by 29.6%. Also, the reduction in losses for electrochromic windows

* Corresponding author: Roohollah Rafee
Faculty of Mechanical Engineering, Semnan University, 35131-19111 Semnan, Iran
Email: rafee@semnan.ac.ir

is 44.7%. In another article, Heidari et al. [3] examined different window configurations for a building in Semnan, Bandar Abbas, and Tabriz cities in a techno-economic analysis. In this paper, heating and cooling demand loads under the different window structures are calculated and compared. The number of window panes, insulation gas between the panes, the thickness of the glass, and the distance between the panes are the decision variables in optimizing the configuration of windows. Chen et al. [4] evaluated multi-objective optimization on the factors affecting the building envelope. The optimization was performed to achieve the values of the decision variables by a genetic algorithm. Decision variables include the heat transfer coefficient of external walls, roof, exterior and interior windows, and the amount of solar energy absorbed by external walls and roof. The results for the optimal structure show a 32.2% increase in thermal comfort and a 10.6% decrease in energy consumption.

Optimization of building energy consumption in addition to considering the design of walls, ceilings, windows, doors, materials, and dimensions, other building characteristics such as occupants, location, HVAC, various forms, and building usage are also included. In a study, Ilbeigi et al. [5] optimized the energy consumption of an office building. Genetic algorithms and ANN are considered tools of optimization. They used EnergyPlus software to evaluate building performance. The results of this study show that energy consumption is reduced by 35% at the optimum point. It can also be seen that the number of inhabitants of the building is the most effective parameter in the energy consumption of the building. Similarly, in another article, Feng et al. [6] optimized energy consumption for different forms of an office building. They used RIUSKA software for simulation and obtained the optimal structure of the building using the Manta-Ray Foraging algorithm. The results of this research show that the uses of rectangular and trapezoidal forms are the closest scenarios to the optimal state. Ebrahimi-Moghadam et al. [7] evaluated the effect of using light shelves in the interior of the building. Thermal comfort and energy consumption are objective functions of the optimization process. The results show a reduction of 111.848kWh of the total consumption of heating, cooling, and electrical loads in the optimal structure.

With the introduction of renewable energy, especially solar energy, and the issue of distributed generation, the use of these systems to supply triple loads to buildings has expanded. Accordingly, many researchers have suggested the use of renewable systems to supply the building loads. Behzadi et al. [8] studied an energy system based on the use of a storage tank and a set of PVT panels for exergy and economic purposes. A genetic algorithm has been used to optimize the system. At the optimum point, 6.7 € / MWh is saved for electricity generation and 7.7 € / MWh for heat generation. Braun et al. [9] proposed the use of PVT panels in a multiple generation system for a zero-energy building. This system has been investigated for three climatic zones. The results of this study show that the use of this system is economically justified for all regions, but government policies have a significant impact on the economic feasibility of using this system. Herrando et al. [10] compared the use of a solar thermal collector, a thermal photovoltaic panel, and a simple photovoltaic panel to supply loads to a University Campus. The results of this study show that the use of a combined system with PVT has the best technical performance, and also the system has the least pollution in this case.

The present study focuses on the energy production sector. The production unit can be designed and implemented for any building and at any stage of building life. This idea can be appropriate in Iran. Because most government and residential buildings are not optimized from the point of view of energy consumption due to their long life and ignoring energy conservation. Three heating, cooling, and electrical loads of a building are provided by the simultaneous production system in most researches. In this regard, we can refer to the article presented by Mago and Smith [11]. In this paper, the cogeneration system is investigated for buildings with different uses. Barbieri et al. [12] investigated the effect of thermal energy storage in a multi-generation system with four primary actuators in a residential building. In an article, Celador et al. [13] demonstrated the economic

superiority of using a cogeneration system over a conventional structure for a residential building. Smith et al. [14] evaluate the importance of using a heat storage unit in a CHP system for several commercial buildings based on energy, environmental and, economic views. Knizley and Mago [15] compared the performance of a multi-generation system with two power units for a restaurant, hotel, hospital, and university. Pirkandi et al. [16] evaluated the effects of design parameters of a gas turbine on the performance of a cogeneration system for a residential building. Kayo et al. [17] studied the load supplying pattern of four combined commercial buildings. Adam et al. [18] investigated the use of fuel cells in a cogeneration system. The goal of this article is to determine the best and closest combination to the zero-energy structure. Liu et al. [19] investigated the performance of a multi-generation system coupled with PV panels for a residential building. Amber et al. [20] presented different scenarios based on heat and electrical load demand, cogeneration system size, etc. for several university buildings in the UK and analyzed them based on life cycle parameters, payback period.

Optimization and analysis of the energy production system in buildings have been considered by many researchers. Lei et al. [21] studied a CCHP system for office buildings and shopping malls. Ashouri et al. [22] used a life cycle assessment pattern. This method is a combination of exergy analysis and life cycle assessment to obtain the appropriate thickness for the walls of a building. Hanifzadeh et al. [23] evaluated and measured a combined production system of cooling, heating, and power for office and commercial buildings. Lu et al. [24] optimized a hybrid renewable energy system for buildings with zero or low energy using multi and single-purpose optimization methods. Recent studies in the field of energy in buildings are divided into three categories. The first group studies building materials and optimizes them to achieve minimal heat, cooling, and electricity losses. The second group aims to design the building's interior equipment to reduce energy consumption. The goal of the third group is to optimize energy production.

The present study aims to design and optimize an integrated energy system for supplying the triple (heating, cooling, and electrical) loads of an educational building. In this research, a case study in Tehran has been simulated by SketchUp, OpenStudio, and EnergyPlus software. Contrary to traditional design, which used the peak loads of the building as criteria for building design, the building is dynamically modeled in this study. Hourly loads of heating, cooling, and electricity are extracted for the building throughout the year. The integrated system designed to supply building loads is a fossil-solar cogeneration system. The system is dynamically modeled, optimized, and analyzed. The optimization was performed in two patterns of three-objective and two-objective. Finally, the optimization results are evaluated and compared based on exergy, economic, and pollution objectives. System and subsystem sizing are performed in all optimization modes. In most previous studies, the off-design conditions were not considered in the optimization process. However, this assumption is incorrect due to the dynamic conditions of weather and building loads. Accordingly, in this article, in addition to sizing the integrated system in the dynamic design mode, the off-design conditions of the subsystems for annual performance are also considered. Highlights and novelties of this article are:

- Comparison of two-objective and three-objective optimization of an integrated fossil-solar energy system
- System sizing in all modes of optimization and evaluation of the effect of considering the objective functions of exergy efficiency, cost rate, and pollution index in the size of each subsystem
- Finding the optimal subsystem size based on off-design system performance
- Considering subsystem performance with changes in air temperature, the capacity of subsystems, and triple building loads
- Investigating the effect of grid connection on subsystem sizes and behavior of integrated energy system with technical, economic, and pollution goals

Nomenclature

A	Area (m^2)
AB	Auxiliary Boiler
$\dot{C}$	Cost Rate ($/s)
C_p	Specific Heat (J/kgK)
CT	Correction Temperature (K)
$\dot{E}$	Exergy Flow Rate (kW)
e	Specific Exergy (kJ/kg)
G	Solar Irradiance (W/m^2)
h	Specific Enthalpy (J/kg)
i	Interest Rate (%)
$\dot{m}$	Mass Flow Rate (kg/s)
N	Operation Time (hour)
P	Pressure (kPa)
$\dot{Q}$	Heat Transfer Rate (W)
R	Gas Constant (kJ/kg.K)
s	Specific Entropy (J/mol)
t	Time
T	Temperature (^oC and K)
U	Overall Heat Transfer Coefficient (W/m^2K)
V	Volume (m3)
$\dot{W}$	Power (W)
x	Molar Fraction
Z_k	Component Purchase Cost ($)
$\dot{Z}_k$	Investment Cost Rate ($/s)

Greek letters

η	Efficiency (%)
φ	Maintenance Factor
ρ	Density (kg/m3)

Abbreviations

CCHP	Combined cooling, Heating, and Power
CF	Cycle Fraction
COP	Coefficient of Performance
CRF	Capital Recovery Factor
EXH	Excess heat
EXP	Excess power
HRB	Heat Recovery Boiler
LHV	Lower Heating Value (kJ/kg)
LMTD	Logarithmic Mean Temperature Difference (^oC)
PLR	Partial Load Ratio
PVT	Photovoltaic Thermal
SC	Solar Collector
ST	Storage Tank

Subscripts

0	Atmospheric Condition
a	Air
ABCH	Absorption chiller
am	Ambient
AV	Average
B	Boiler
BE	Bought Electricity
c	Cooling Load
cond	Condenser
D	Design mode
DEM	Demand
E	Electrical Load
Elec	Electricity
evap	Evaporator
f	Fuel
g	Gas
Gen	Generator
GT	Gas Turbine
H	Heating load
HEX	Heat exchanger
i	Inlet
max	Maximum
Nom	Nominal
o	Outlet
op	Operational Condition
PV	Photovoltaic Cells
PVT	Photovoltaic Thermal
s	steam
sat	Saturate
SC	Solar Collector
SE	Sold Electricity
sq	Steam quality
ST	Storage Tank
w	water

Superscripts

CH	Chemical
CI	Component Investment
KN	Kinetic
OM	Operation And Maintenance
PH	Physical
PT	Potential

2.System description

The model studied in the present study is an educational building in Tehran. The building is designed on six floors (Fig.1). The area of the building floors is 10452 m^2. The building has been designed, simulated, and analyzed by SketchUp, OpenStudio, and EnergyPlus software, and the required dynamic loads have been extracted. The cooling, heating, and electrical loads of the building are obtained on an hourly basis, according to Fig. 2. The assumptions of building and analysis of the studied integrated energy system are presented in Table 1.

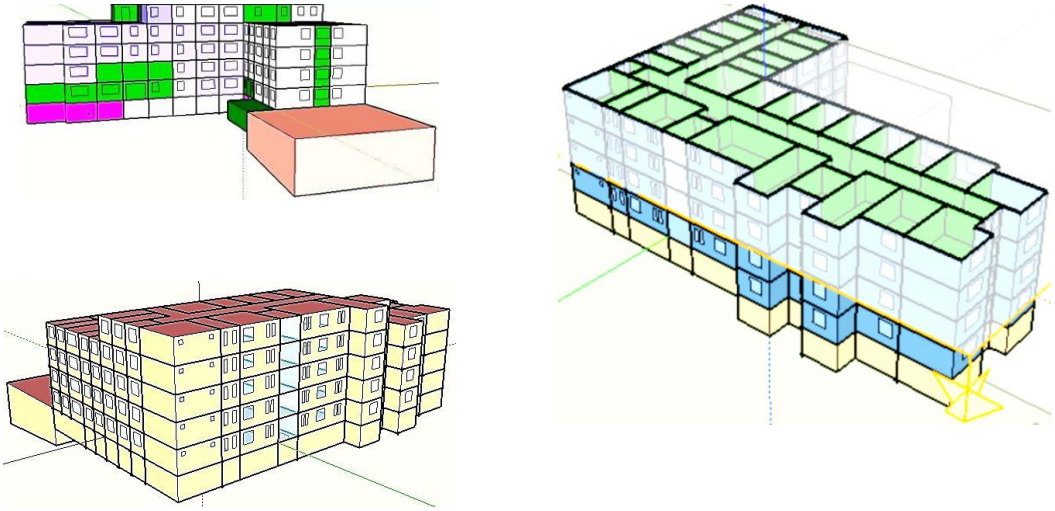

Fig. 1. Schematic of building in SketchUp software

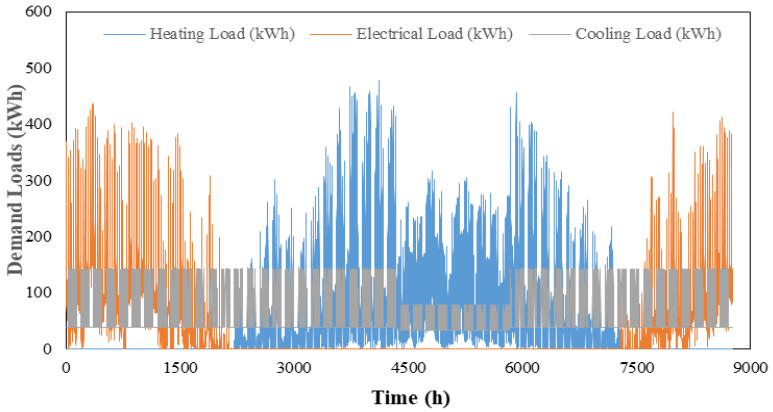

Fig. 2. Dynamic cooling, heating, and electrical loads of modeled educational building

Table 1. Assumptions of modeling and analysis of building and integrated energy system

Variables	Type/Value
Discount Rate	18%
System analyzing period	20 years
Building characteristics:	
Environment location	Tehran
Building type	Secondary School
Number of floors	6
Total area	10452 m^2
Total glass area	752.06 m^2
External wall overall U-value	4.980 (W/m^2K)
Internal wall overall U-value	5.853 (W/m^2K)
Windows overall U-value	5.327 (W/m^2K)
Roof overall U-value	0.223 (W/m^2K)
Floor overall U-value	2.945 (W/m^2K)
Used standard	ASHRAE-2019
Electricity price:	
Intermediate load hours	414 Rial/kWh
Peak load hours	828 Rial/kWh
Low load hours	207 Rial/kWh
Natural Gas:	
price for office buildings in cold period (Nov 06--- Apr 04)	1495 Rial/m^3
price for office buildings in warm period (Apr 05 --- Nov 05)	2990 Rial/m^3
Fuel LHV	36000 kJ/std m^3

The integrated energy system consists of two parts of fossil and solar subsystems (Fig. 3). Generate electricity is the main task of a gas turbine in an integrated energy system. Gas turbine exhaust heat can be recovered by the HRB and used in the heating part of the building. PVT is also used to supply electricity. The use of water pipes behind the panels of this subsystem, in addition to providing part of the heat, can also raise the efficiency of the panels. The solar collector is also exploited to help supply the required heat. Due to the dynamic performance of the subsystems and the building, the system is faced with a lack or excess of heat during the hours of a year. The demand heat is the summation of the heating load of the building and the heat required by the absorption chiller generator. The excess heat is sent to the storage tank. When the heat generated by the upstream subsystems, i.e., solar collector, PVT, and heat recovery boiler, is less than the demand of the building, the use of the storage tank is the priority. If the storage tank is completely discharged, the heat lack will be provided by an auxiliary boiler. There is a similar procedure for system power generation and building consumption. Accordingly, the connection with the grid is considered for buying and selling electricity. When the electricity produced by the system is more than the building consumption, this electricity is sold to the grid. If the electricity produced by the system is less than the required amount of the building, the electricity shortage is supplied by purchased from the grid.

3.Modeling

After calculating the triple loads of the building, the values of the decision variables are randomly selected based on the lower and upper bounds. These decision variables are the design parameters and size of the subsystems. By determining the size of the gas turbine, its production capacity and recoverable heat can be calculated for each hour of the year. Also, the heat generated by the solar collector, and electricity/heat of PVT are calculated for all hours of the year. In this case, the excess heat and electricity are determined per hour. Excess power is the total power generated by a gas turbine and PVT minus the building's electricity consumption. If the value obtained for this phrase is positive, there is a surplus of electricity, and the excess electricity is sold to the grid.

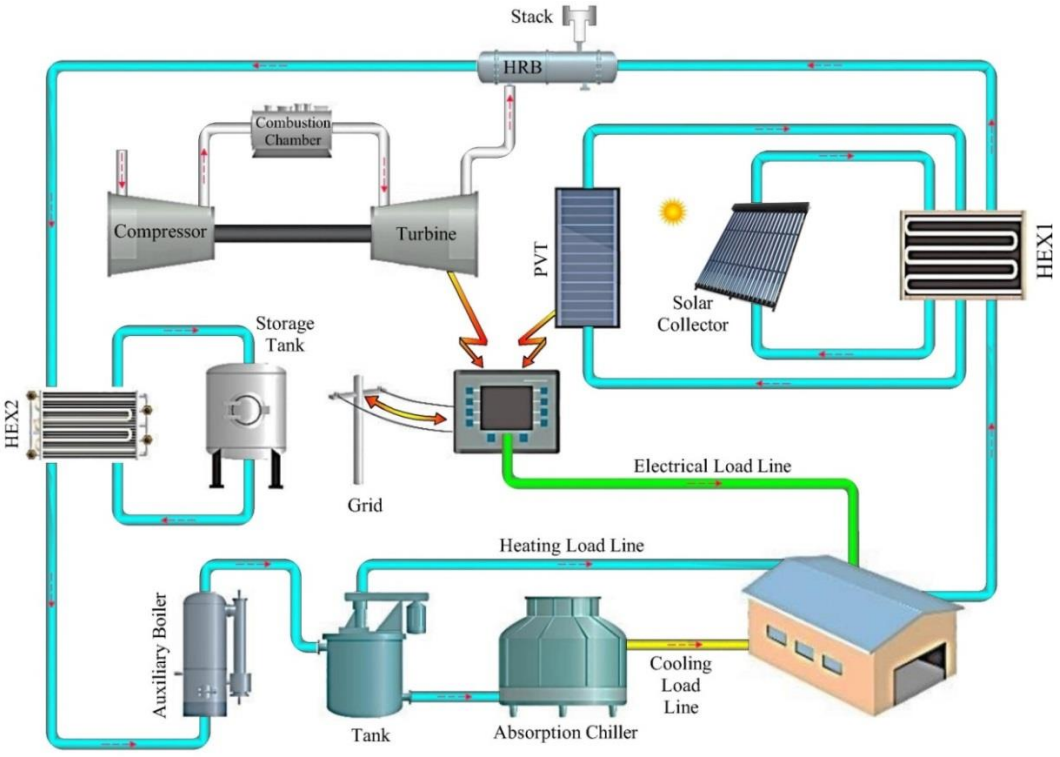

Fig. 3. Configuration of integrated energy system

If the value obtained is negative, the system needs to purchase electricity from the grid. Excess heat is also the sum of heat generated in the solar collector, PVT, and recovered heat of the gas turbine minus the total heat load of the building and the heat required by the absorption chiller generator. If this positive numerical expression is obtained, it means that there is extra heat. In this case, the excess heat is sent to the storage tank. If the value obtained is negative, the system needs heat compensation. This heat is first extracted from the storage tank, and if all the heat is not supplied by the storage tank, the auxiliary boiler compensates for the lack of heat. The modeling flowchart of the studied integrated energy system is shown in Fig. 4.

3.1.Gas Turbine

Off-design behavior means calculating output power, exhaust gas temperature, and fuel and exhaust mass flow rate. The reasons for deviating from the design point in gas turbines are mainly changes in ambient temperature and the required load. The reference point in the estimation and design of gas turbines is the standard conditions (T_{am}= 15 °C, P_{am}=1 atm, and Full load operation). Any deviation from the standard conditions will change the performance of the turbine. The off-design operation of the gas turbine is shown in Figs. 5 to 6. The data presented in Fig. 5 are related to the system's operation in the off-design mode by changing the air temperature. The horizontal axis in this diagram is the temperature change relative to the design mode temperature of 15 °C. The vertical axis also shows the percentage of changes in various parameters such as net output power, thermal efficiency, and exhaust temperature of gas turbine smoke affected by changes in ambient temperature [25]. Similarly, Fig.6 shows the changes for exhaust gas flow and fuel flow based on the distance from the design temperature.

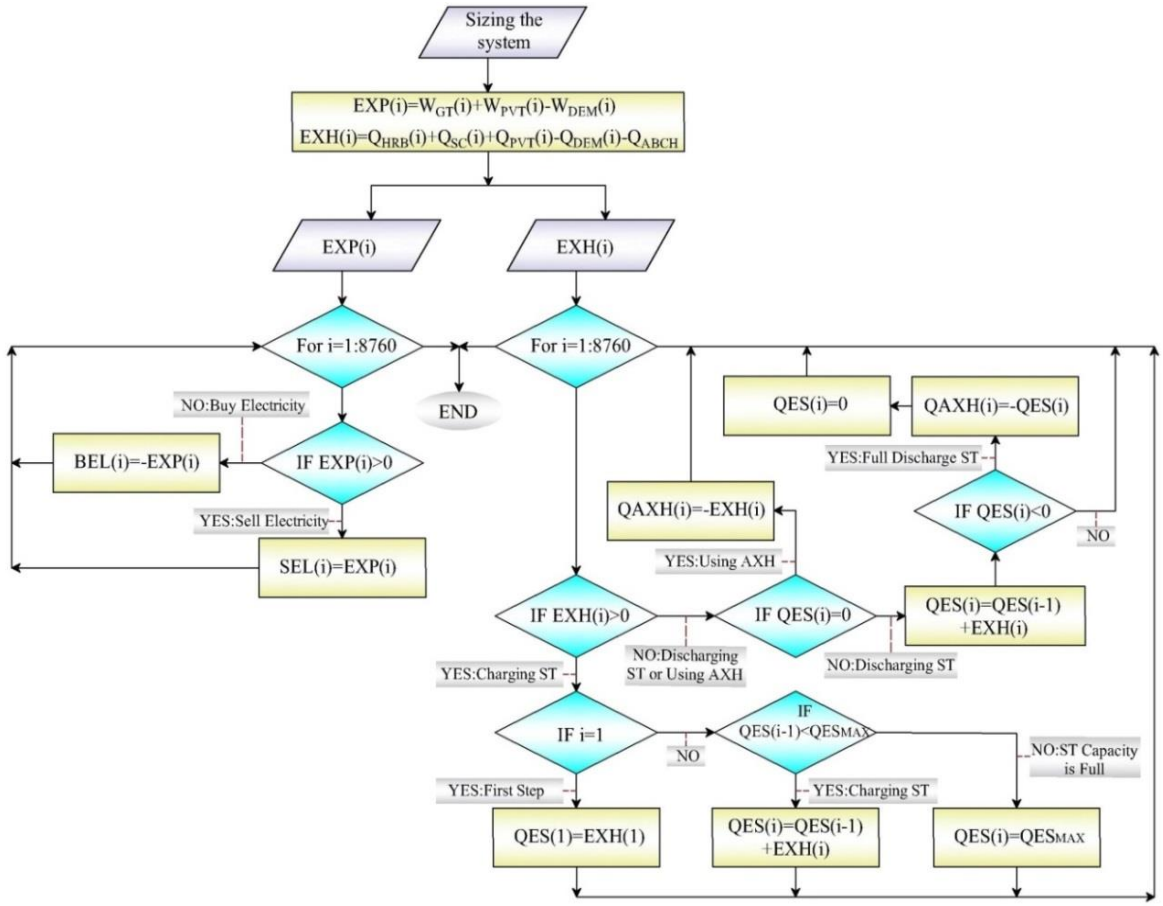

Fig. 4. Flowchart of modeling and simulation process

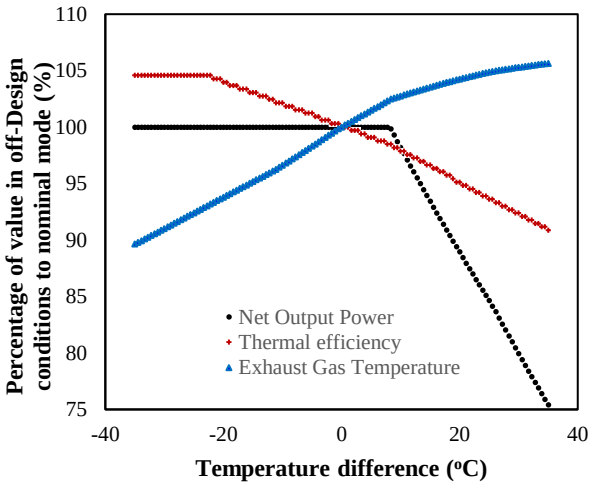

Fig.5. Off-design performance curve of gas turbine with the change of inlet air temperature (gas turbine power, thermal efficiency, and Exhaust temperature)

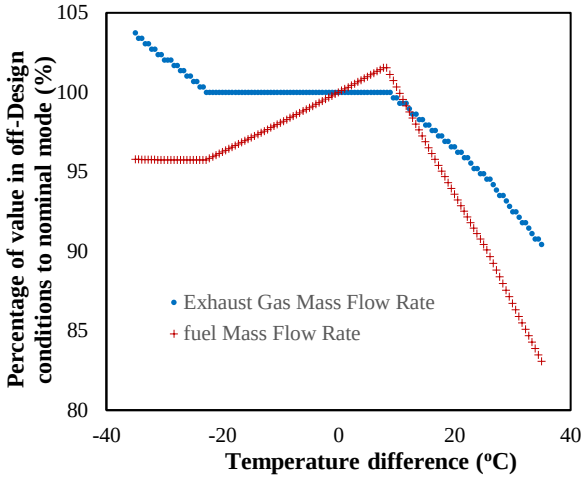

Fig. 6. Off-design performance curve of gas turbine with the change of inlet air temperature (Fuel and exhaust flow)

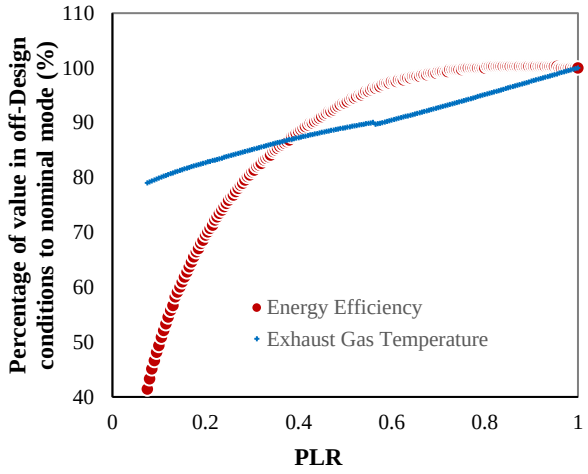

Fig. 7. Off-design performance curve of gas turbine with the changing load (gas turbine power, thermal efficiency, and Exhaust temperature)

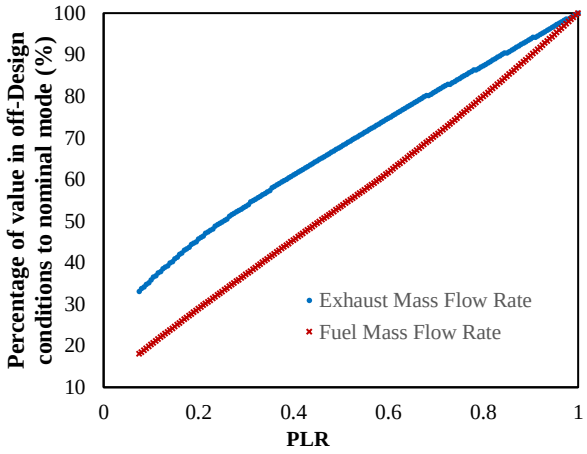

Fig. 8. Off-design performance curve of gas turbine with the changing load (Fuel and exhaust flow)

In addition to ambient temperature, changes in demand load affect turbine outputs. Figures 7 and 8 show the off-design operation of the gas turbine for demand load changes. Fractures in performance curves are due to changes in the behavior of the gas turbine control system. Due to the control constraints, the control system has shown different behavior in different intervals of temperature change and loading, which offers its change curve.

The maximum power available for the gas turbine at ambient temperature is calculated to evaluate the performance of the gas turbine. According to the demand power, the amount of partial load is calculated [25]:

$$PLR_B = PLR \times \frac{W_{Nom}}{W_{max}} \quad (1)$$

Using the partial load percentage, the correction factor for the partial load is calculated. Finally, the specifications of different gas turbine parameters are obtained based on Eq. (2) [25]:

$$A = A_N Cr_{\Delta T} Cr_{PLR} \quad (2)$$

In the above equation, A is the parameter under consideration, such as net power output,

energy efficiency, temperature and mass flow rate of exhaust gas, and mass flow rate of fuel. N is the value of this parameter in the design conditions, Cr is the correction coefficient obtained from Figs. 5 and 6, and Cr is the correction coefficient obtained from Figs. 7 and 8. These correction coefficients are the same percentage of deviation from the gas turbine design mode.

3.2. Heat Recovery Boiler

The recovery exchanger is used at the output of the gas turbine to generate steam or hot water. The hot exhaust gases give off their heat to the water after entering the HRB.

The size of the recovery boiler is selected based on water temperature. The sizing of this equipment determines the UA and the flow rate of the feedwater passing through the heat recovery boiler in design mode. Using Eq. (3), the heat dissipated from the gas flow passage is calculated:

$$Q_{HRB} = m_g C_p \left(T_{gi} - T_{go}\right) \tag{3}$$

Also, the Logarithmic mean temperature difference in the HRB is obtained by Eq. (4) [26]:

$$LMTD_D = \frac{\left(T_{g_{in}} - T_{sat}\left(P_W\right) - \left(T_{g_o} - T_{W_i}\right)\right)}{ln\left(\frac{\left(T_{g_i} - T_{sat}\left(P_W\right)\right)}{\left(T_{g_o} - T_{W_i}\right)}\right)} \tag{4}$$

The total heat transfer coefficient of the recovery boiler in the design mode is calculated using the following Equation [26]:

$$(UA)_D = \frac{Q_{HRB}}{LMTD_D} \tag{5}$$

The second design parameter in this section is the feedwater flow through the HRB, which is obtained by Eq. (6):

$$m_s = \frac{Q_{HRB}}{\left(h_s\left(sq, P_W\right) - h_{W_i}\right)} \tag{6}$$

Off-Design modeling of HRB has been evaluated in some references [27] similar to the boiler system and some other cases [28] as a heat exchanger. The simple model used in this research considers the recovery boiler as a gas-steam exchanger [29]. First, the inlet and outlet temperature values for the water and gas in the heat recovery boiler are extracted at design mode. Using these values, the heat transfer capacity will be as follows [29]:

$$Q_D = \left(U \times A\right)_D \times \left(LMTD\right)_D = \left[\left(m\left(h_o - h_i\right)\right)_w\right]_D \tag{7}$$

In the above Equation, U, A, and LMTD are the exchanger surface, effective conductivity, and logarithmic mean temperature difference, respectively. Index D indicates design conditions. This equation is always true in all off-design points. In off-design situations, the following equations have been used to correct the UA [29]:

$$UA_{op} = \frac{\left(m_g^{0.65} F_g\right)_{op}}{\left(m_g^{0.65} F_g\right)_D} UA_D \tag{8}$$

$$F_g = \frac{Cp^{0.33} k^{0.67}}{\mu^{0.32}} \tag{9}$$

According to the energy and mass conservation equations, the HRB equations can be solved, and the production capacity can be estimated in different off-design conditions.

3.3. Auxiliary Boiler

After calculating the heat recovered by HRB, the auxiliary boiler size can be calculated from the following equation [30]:

$$Q_B = \max\left(Q_{H_{Dim}} - Q_{HRB}, Q_{Gen} - Q_{HRB}\right) \tag{10}$$

The above calculation is an unsafe estimate. In real models, the auxiliary boiler is designed to consider the full production capacity (considering the conditions that the HRB will not be in the circuit). In this case, the size of the boiler is [30]:

$$Q_B = \max\left(Q_{H_{Dim}}, Q_{Gen}\right) \tag{11}$$

The system with the above design will be off-design in most cases. Therefore, to prevent the reduction of boiler efficiency in different operating conditions, usually two or more boilers are used that have less and similar capacity. Boiler efficiency is the amount of heat transferred to water relative to the energy consumed by the fuel. Off-design conditions usually occur due to changes in mass flow rate and temperature of boiler inlet water. The sensitivity of the boiler efficiency to the inlet water temperature is low, especially at high loads, because the hot gas stream enters with a high combustion temperature, which LMTD can

be estimated almost independently of the inlet water temperature changes. The third order Eq. (12) is used to estimate the change in boiler efficiency in the off-design conditions [31]:

$$\frac{\eta_{op}}{\eta_D} = a_1 + a_2 PLR + a_3 PLR^2 + a_4 PLR^3 \quad (12)$$

$$PLR = \frac{Q_{op}}{Q_D} \quad (13)$$

The fixed numbers in this equation are defined in Table 2.

Table 2. Fixed coefficients related to Equation (12)

a_1	a_2	a_3	a_4
0.011771251	0.98061775	0.11783017	-0.11032275

3.4. Absorption Chiller

The amount of heat load required by the absorption chiller is:

$$Q_{Gen} = \frac{Q_{C_D}}{COP_D} \quad (14)$$

The off-design calculations of the absorption chiller are more complex than the boiler, HRB, and turbine. Because the performance of the absorption chiller depends on three off-design parameters with different natures. These parameters are:

- Environmental conditions that affect condenser and building load
- The building load that affects the temperature and flow of water entering the evaporator and determines the amount of cooling load required
- Changing in mass flow rate and inlet steam temperature to the absorption chiller generator which is a function of the conditions of the HRB or auxiliary boiler

Chiller design equations are presented by ASHRAE and DOE-2 relations [31-33]. In this model, a set of correction coefficients and factors are used. The absorption chiller used here is an indirect single-effect water–LiBr absorption chiller that works with hot water or low-temperature steam. The partial load of the absorption chiller in the off-design conditions is defined by the following relation:

$$PLR = \frac{\left(Q_{evap}\right)_{op}}{\left(Q_{evap}\right)_{max}} \quad (15)$$

The load of the evaporator is the same as the cooling load of the building in the operating conditions. The maximum evaporator load is calculated using a set of correction relationships. The first correction equation is related to the evaporator temperature, which is presented below [32]:

$$CT_{evap} = \sum_{i=1}^{4} a_i T_{evap}^{i-1} \quad (16)$$

The second correction equation is related to the condenser temperature correction. Condenser temperature refers to the temperature of the water entering the condenser (water cooler) [32].

$$CT_{cond} = \sum_{i=1}^{4} b_i T_{cond}^{i-1} \quad (17)$$

The third correction factor is related to the temperature of the heat source entering the generator [32]:

$$CT_{gen} = \sum_{i=1}^{4} c_i T_{gen}^{i-1} \quad (18)$$

The maximum production refrigeration capacity can be calculated by the following equation [32]:

$$\left(Q_{evap}\right)_{max} = CT_{evap} \times CT_{gen} \times CT_{cond} \times \left(Q_{evap}\right)_{rated} \quad (19)$$

The same equations are used to estimate the generator temperature as follows. In the first step, the partial load correction factor must be calculated [32]:

$$GHIR = \sum_{i=1}^{4} d_i \, PLR^{i-1} \quad (20)$$

Changing the temperature of the inlet heat source (hot water) can also cause the absorption chiller to be off-design. The following equation is used to calculate it [32]:

$$GT_{gen} = \sum_{i=1}^{4} e_i \, T_{gen}^{i-1} \quad (21)$$

Changing the evaporator temperature can also change the heat load required by the chiller. Equation (22) is intended for this purpose [32]:

$$GT_{evap} = \sum_{i=1}^{4} f_i \, T_{evap}^{i-1} \quad (22)$$

T_{Evap} is the temperature of the water leaving the evaporator.

The condenser temperature correction factor is also presented with a similar equation [33]:

$$GT_{cond} = \sum_{i=1}^{4} h_i T_{cond}^{i-1} \tag{23}$$

At low cooling loads, the absorption chiller switches continuously between on and off states. For this purpose, the cycle fraction correction factor is used [33]:

$$CF = \min\left(1, \frac{PLR}{PLR_{min}}\right) \tag{24}$$

The required heat of the generator is estimated as follows using the previous correction coefficients [33]:

$$Q_{gen} = GHIR \times GT_{gen} \times GT_{evap} \times CF \times \left(Q_{evap}\right)_{max} \tag{25}$$

The temperature correction coefficient of the generator is 1 when steam is used as the generator of the absorption chiller. Table 3 presents the data and coefficients used for the above relationships.

3.5. Storage Tank

The storage tank is modeled assuming complete mixing. Therefore, the fluid inside the tank is considered isothermal. The governing equation for tank dynamics modeling is written as shown in Fig. 9 [34]:

$$\frac{dE_{C.V}}{dt} = -\dot{Q}_r + \dot{m}_{user} h_{out,user} + \dot{m}_{sol} h_{sol} - \dot{m}_{user} h_{hot,out,ST} - \dot{m}_{sol} h_{cold,out,ST} \tag{26}$$

The discrete modeling relationship to achieve the average storage tank temperature is [34]:

$$T_{AV}^{P+1} = \left[\left(\frac{\dot{m}_{sol}}{\rho V_{ST}} T_{sol} + \frac{\dot{m}_{user}}{\rho V_{ST}} T_{out,user} + \frac{U\left(A_{ST,sid} + A_{sec}\right)}{\rho C_p V_{ST}} T_a\right) - \left(\frac{\dot{m}_{sol}}{\rho V_{ST}} + \frac{\dot{m}_{user}}{\rho V_{ST}} + \frac{U\left(A_{t,sid} + A_{sec}\right)}{\rho C_p V_{ST}}\right) T_{AV}^{P}\right] \Delta t + T_{AV}^{P} \tag{27}$$

3.6. PVT and Solar Collector

Modeling of photovoltaic panel and solar collector is similar to reference [35]. In the present study, the temperature of each layer is assumed to be constant and the conductive heat transfer in each layer of the panel and collector is neglected.

Table 3. Fixed coefficient values in off-design modeling of absorption chiller design

i	a	b	c	d	e	f	h
1	0.690571	0.245507	1	0.18892	1	0.995571	0.712019
2	0.065571	0.023614	0	0.968044	0	0.046821	-0.00478
3	-0.00289	2.78E-05	0	1.119202	0	-0.01099	0.000864
4	0	1.30E-05	0	-0.5034	0	0.000608	-1.30E-05

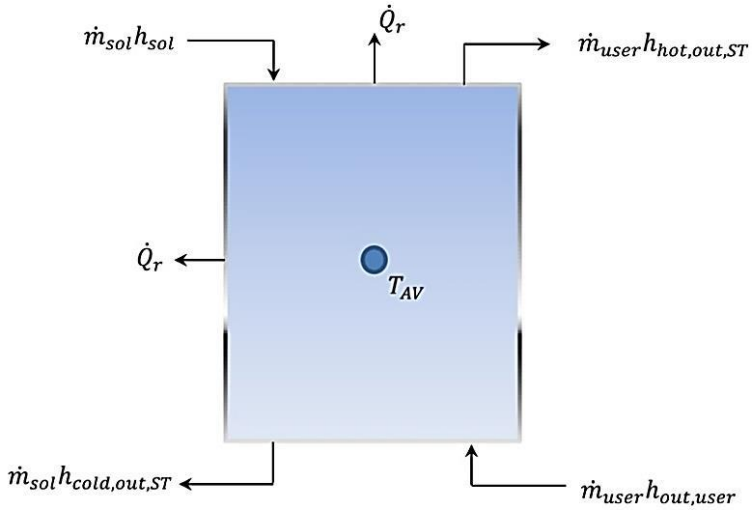

Fig. 9. Simple volume control model for simultaneous charging and discharging of storage tanks

3.7.Exergy Analysis

The results of exergy analysis are more accurate than the energy analysis for a thermal system. Exergy generally consists of four components, which are as follows [36]:

$$e=e^{PH}+e^{CH}+e^{PT}+e^{KN} \quad (28)$$

The studied integrated system is stagnant relative to the environment, so kinetic and potential exergy can be ignored. Physical exergy is the distance between the temperature and pressure of the fluid to the dead state. The following equation is used when the fluid is liquid or vapor [37]:

$$e^{PH}=\left(h-h_0\right)-T_0\left(s-s_0\right) \quad (29)$$

The following relation can be proved for gases [38]:

$$e^{PH}=C_p\left[T-T_0-T_0 ln\left(\frac{T}{T_0}\right)\right]+RT_0\left(\frac{P}{P_0}\right) \quad (30)$$

The chemical exergy of combustion products is calculated as follows [39,40]:

$$e^{CH}=-RT_0\sum_{i=1}^{k}x_i ln\left(\frac{x_i^e}{x_i}\right) \quad (31)$$

For hydrocarbon fuels, chemical exergy can be defined as Equation (32). In this relation, a and b are the number of carbon and hydrogen in the chemical relation of the desired fuel (C_aH_b), respectively [41-43].

$$e_f^{CH}=LHV.\gamma_f \quad (32)$$

$$\gamma_f=1.033+0.0169\frac{b}{a}-\frac{0.0698}{a} \quad (33)$$

In the above equations, γ_f and LHV are exergy grade function and lower heating value of the fuel, respectively [44,45].

Equation (34) represents the exergy efficiency of the proposed integrated energy system:

$$\eta_{ex}=\frac{\sum_{i=1}^{8760}\left(E_H+E_C+W_E+W_{SE}\right)}{\sum_{i=1}^{8760}\left(E_{in,PVT}+E_{in,SC}+E_f+W_{BE}\right)} \quad (34)$$

The constituent parameters of above equation are defined as follows:

$\dot{E}_H$ is the exergy of heat production, which is equal to the heat load of the building during a year and is obtained from Fig. 2. $\dot{E}_C$ is the exergy cooling production, which is equal to the cooling load of the building during one year and is obtained from Fig. 2. $\dot{W}_E$ is the electricity required by the building, which must be supplied by the integrated energy system and the grid and obtained from Fig. 2. $\dot{W}_{SE}$ is the total electricity sold to the grid for a year calculated in the optimization procedure. $\dot{W}_{BE}$ is the total power purchased from the grid, which is obtained in the optimization procedure. $\dot{E}_f$ is the exergy of fuel consumption in gas turbines and auxiliary boilers, which is calculated from the product of the mass flow of fuel consumed in the chemical exergy of fuel as follows:

$$E_f=m_f e_f^{CH} \quad (35)$$

$\dot{E}_{in,SC}$ and $\dot{E}_{in,PVT}$ are the input exergy to the solar collector and PVT from the sun which is obtained from relations 36 and 37, respectively [46]:

$$E_{in,SC}=GA_{SC}\left(1-\frac{T_{am}}{T_{AV,SC}}\right) \quad (36)$$

$$E_{in,PVT}=GA_{PVT}\left(1-\frac{T_{am}}{T_{AV,PVT}}\right) \quad (37)$$

3.8. Economic Analysis

The total cost per kWh of electricity generated is calculated by the following equation [47]:

$$C_{total}=C_{fuel}+Z_{total}-C_{Elec,sell}+C_{Elec,buy} \quad (38)$$

The cost of fuel consumed by the system is defined as follows [48]:

$$C_{fuel}=\left(c_{fuel}m_{fuel}LHV\right)*3600 \quad (39)$$

$\dot{Z}_{total}$ is the cost of purchasing equipment, which is obtained from equations (40) and (41) [49-51]:

$$Z_{total}=Z_k^{CI}+Z_k^{OM}=\frac{\varphi\sum\left(Z_k*CRF\right)}{N} \quad (40)$$

$$CRF=\frac{i(1+i)^n}{(1+i)^n-1} \quad (41)$$

$\dot{Z}_k^{OM}$ and $\dot{Z}_k^{CI}$ are the cost of operation & maintenance and the purchasing of integrated system equipment, respectively. Z_k is the initial price of the equipment, that is

considered according to the reference [47] and presented in Table 4.

3.8. Pollution index

Pollution index is a function of CO_2 production and total heat, cooling, and electricity production and is defined as follows [47]:

$$EMI = \frac{m_{tot,CO2}}{Total\ Load} \quad (42)$$

4. Results and discussion

The integrated energy system is modeled by MATLAB software, and the genetic algorithm has been used for optimization. Exergy efficiency, total cost rate, and pollution are considered optimization objective functions. The optimization is done in the mode of two and three objectives (Figs. 10 to 17). The lower and upper bounds of decision variables in the optimization process are presented in Table 5.

Table 4. Capital price of integrated energy system equipment

Component	Capital Price
Air Compressor	$Z_{AC} = \left(\frac{71.1 m_{air}}{0.9 - \eta_{AC}}\right)\left(\frac{P_{12}}{P_{11}}\right) ln\left(\frac{P_{12}}{P_{11}}\right)$
Combustion Chamber	$Z_{CCh} = \left(\frac{46.08 m_{air}}{0.995 - \frac{P_{13}}{P_{12}}}\right)\left[1\_exp(0.018 T_3 - 26.4)\right]$
Turbine	$Z_{GT} = \left(\frac{479.34 m_{gas}}{0.92 - \eta_{GT}}\right) ln\left(\frac{P_3}{P_4}\right)$
Flat-Plate Solar Collector	$Z_{FPC} = 235 A_{FPC}$
Photovoltaic/Thermal	$Z_{PVT} = 1000 A_{PVT}$
Auxiliary Boiler	$Z_{AB} = Q_{AB}\left(1215.8 Q_{AB}^{-0.4827}\right)$
Thermal Energy Storage	$Z_{TES} = 4042 V_{TES}^{0.506}$
Heat Exchanger	$Z_{HEX} = 130\left(\frac{A_{HEX}}{0,093}\right)^{0.78}$
Absorption Chiller	$Z_{HEX} = 1144.3\left(Q_{EVA}\right)^{0.67}$

Table 5. The lower and upper bound of decision variables

	Storage Capacity (kWh)	Collectors Area (m^2)	GT Power (kW)	PVT Rows
Lower Bound	0	0	0	0
Upper Bound	10000	800	400	70

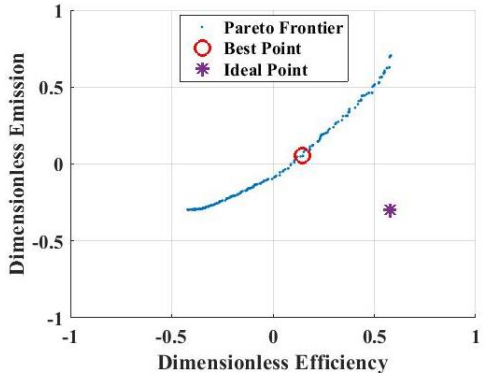

Fig. 10. Two-objective and dimensionless Pareto diagram with the objective functions of pollution index and exergy efficiency

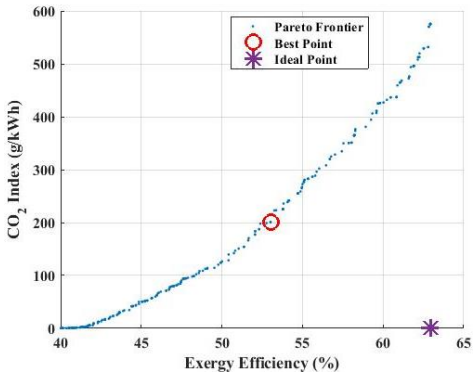

Fig. 11. Two-objective Pareto diagram with the objective functions of pollution index and exergy efficiency

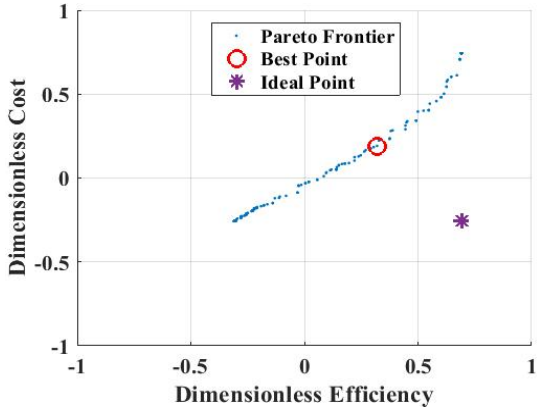

Fig. 12. Two-objective and dimensionless Pareto diagram with the objective functions of total cost rate and exergy efficiency

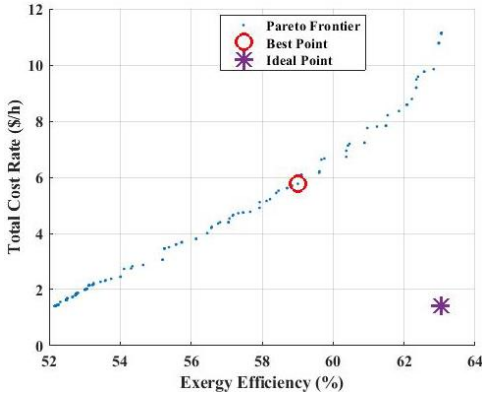

Fig. 13. Two-objective Pareto diagram with the objective functions of total cost rate and exergy efficiency

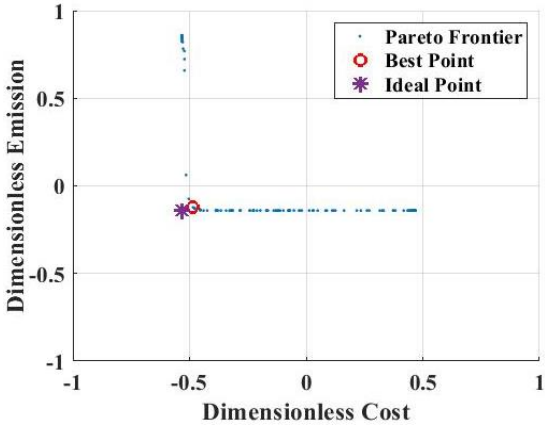

Fig. 14. Two-objective and dimensionless Pareto diagram with the objective functions of pollution index and total cost rate

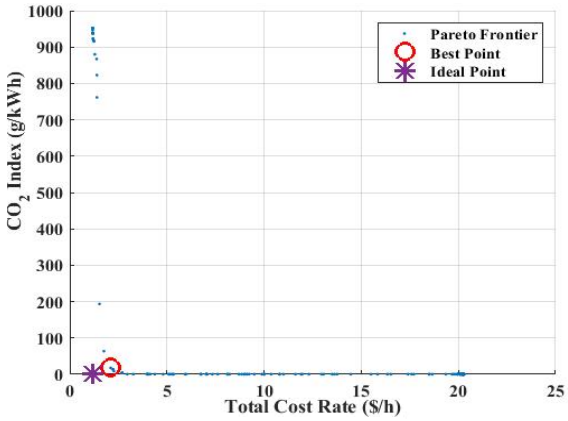

Fig. 15. Two-objective Pareto diagram with the objective functions of pollution index and total cost rate

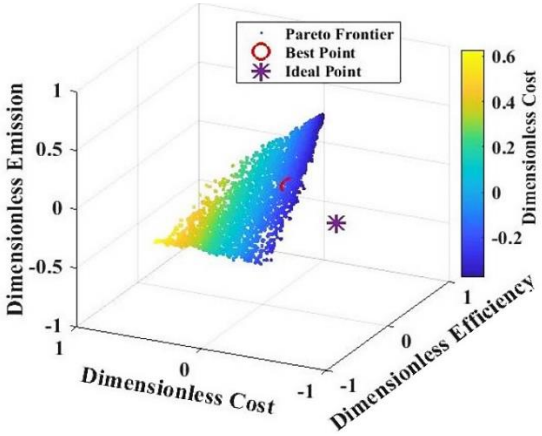

Fig. 16. Three-objective and dimensionless Pareto diagram with the objective functions of exergy efficiency, pollution index and total cost rate

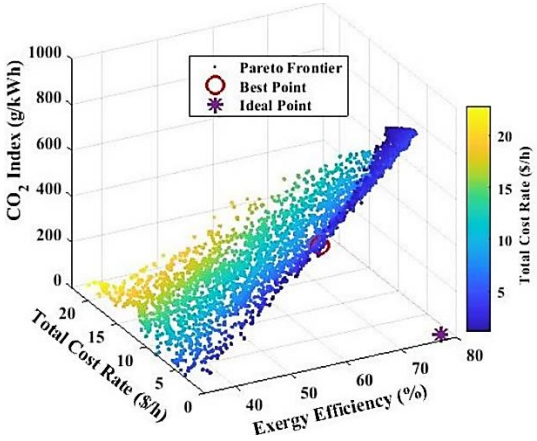

Fig. 17. Three-objective Pareto diagram with the objective functions of exergy efficiency, pollution index and total cost rate

Figures 10 and 11 show the two-objective optimization of the integrated energy system with the objective functions of exergy efficiency and pollution. Optimization has been done to maximize exergy efficiency and minimize CO_2 emissions. Figure 10 is the dimensionless state of Fig. 11. It is necessary to use a dimensionless diagram to determine the optimal performance point. In the Pareto dimensionless diagram, the best performance point of the two-objective is the closest point to the equilibrium situation. The equilibrium point is the state with the minimum pollution and the maximum exergy efficiency. In this case, the exergy and pollution efficiencies are 53% and 200.9 g/kWh, respectively. Also, the total cost is less important and is 20.6 $/h. Table 6 shows that this mode of optimization has the highest total cost rate. The second optimization method is proposed with the two goals of maximizing exergy efficiency and minimizing cost. Undoubtedly, pollution is less important in this case. In this case, the pollution index and the exergy efficiency are 767 g/kWh and 59%, respectively. Comparing Figs. 12 and 13 with the previous two graphs, it can be seen that achieving a lower pollution index has less effect on reducing system efficiency than reducing the total cost. The total cost rate in this scenario is 5.77 $/h. Comparing the proposed scenarios, it can be seen that the lowest cost and pollution rates were equal to 2.1 $/h and 171 g/kWh, respectively, which occurred in the optimization model with two objectives of reducing costs and pollution (Figs. 14 and 15). The important point in this method is the large reduction in efficiency of the integrated energy system. It can be seen that the highest efficiency drop is related to this scenario, and the exergy efficiency has reached 37.88%. Considering the importance of the goals of increasing exergy efficiency, reducing cost rate and pollution, three-objective optimization of the system is important. This model introduces the best three-objective performance of the system. Although the exergy efficiency in this scenario is 50.21% (Figs. 16 and 17), and this value is lower compared to the first and second scenarios, it can be seen that the pollution and the total cost rate are more reasonable values. The pollution produced and total cost rate are 301 g/kWh and 7.1 $/h in this method.

Figures 18 and 19 show the exergy efficiency is more sensitive to pollution changes. For points with a fixed cost rate, the slope of the exergy efficiency changes relative to the pollution index represents the mutual influence of these parameters. The effect of exergy efficiency and total cost rate can be analyzed based on the slope of changes for points with constant pollution. The results show that the slope of changes in Fig. 19 is higher. Therefore the exergy efficiency is more affected by the objective function of the pollution index. Exergy efficiency is affected by many parameters such as the electricity purchased from the grid. This parameter also is influential in the total cost rate. The results of Table 7 show the maximum purchased electricity is accrued in the optimization with the goals of exergy efficiency and cost. In this case, 501.9 MWh of electricity is purchased from the grid for one year. This is due to the cheap price of electricity in Iran. The lowest electricity sale occurred in this scenario that is 5.26 MWh.

Table 6. Size of the integrated energy system and values of objective functions for evaluated scenarios

Objective functions	PVT Rows	SC Area (m^2)	ST Capacity (kWh)	GT Power (kW)	Exergy Efficiency (%)	Total Cost Rate ($/h)	CO_2 Index (g/kWh)
Efficiency & Emission	68	6.25	3774	26.88	53.02	20.6	200
Efficiency & Total cost	17	6.75	75.21	10.45	59.01	5.77	767
Total cost & Emission	1	11.8	17.85	131.1	37.88	2.10	171
Efficiency & Total cost & Emission	20	5.27	462.5	37.43	50.21	7.10	301

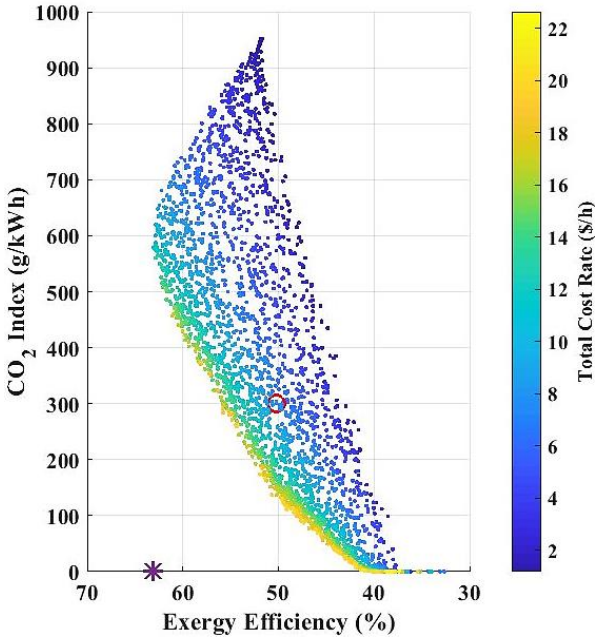

Fig. 18. Interaction between exergy efficiency and CO_2 emission index

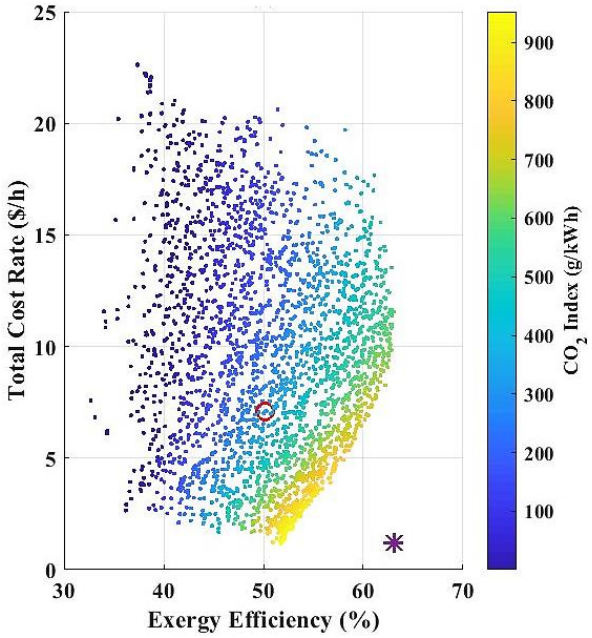

Fig. 19. Interaction between exergy efficiency and total cost rate

The use of renewable energy has zero CO_2 emissions, so these systems are prevalent in the home sector. The results show that these systems rarely are used. The highest use of PVT was 68 rows, which occurred in a two-objective optimization scenario with exergy and pollution efficiency goals. Pollution reduction is the most important reason for the use of this equipment in the integrated energy system. The value of this parameter is minimal when the cost rate is more important. The results also show that the volume of storage tanks increases when more solar systems are used. The choice of storage tank capacity depends on various parameters that can only be achieved by optimization. The highest capacity obtained for the storage tank is received in the first scenario, i.e., optimization with aim of exergy efficiency and pollution index. In this case, the number of rows of PVT panels is much higher than rows in other scenarios. Accordingly, significant heat is generated by this system in this case. Each row of blades consists of 10 panels with an area of $1m^2$. The capacity obtained for the storage tank, in this case, is 3774 kWh. In addition to optimization and objective functions effects, other variables such as solar collector area and gas turbine capacity are the most critical parameters affecting tank capacity. Using PVT has reached the maximum allowed due to the lack of cost constraints in this scenario. The calculated capacity of the gas turbine is 26.88 kWh.

Table 7. Results of integrated energy system optimization with different objective functions

Objective functions	Boiler size (kWh)	Electricity sold (MWh)	Purchased electricity (MWh)	Boiler heat (MWh)	ST Heat (MWh)	Solar Heat (MWh)	Solar Power (MWh)
Efficiency & Emission	565.4	254.5	155.8	162.8	13637	1945.9	484.5
Efficiency & Total cost	661.1	5.260	501.9	677.7	145.7	486.14	119.4
Total cost & Emission	480.7	551.9	16.04	139.8	158.5	50.354	8.798
Efficiency & Total cost & Emission	575.5	55.05	204.2	288.4	2300	583.06	144.1

In this scenario, the use of solar resources is a priority to supply electricity and heat. PVT provided 484.5 MWh of the building's electricity needs over a year, which is significantly more than other scenarios. The total electricity purchased from the grid is 155.8 MWh, and the total electricity sold in the year is 254.5 MWh. These values are related to the hours when the system cannot generate the required electricity for the building, or the electricity generation of the integrated fossil-solar system is more than the consumption of the building. The lowest heat generated in the boiler also occurs in this scenario and is 162.8 MWh. This is due to the high capacity of the storage tank and the heat absorbed in it. The boiler is responsible for providing the lack of heat generated by the system. There is less need for heat generated by the boiler, and a significant amount of heat is supplied by the storage tank. In this scenario, 1945.9 MW of heat is generated by solar systems throughout the year, which is more than other scenarios.

One of the objectives of this study is to match the obtained results with the real conditions of existing buildings in Iran. Accordingly, government support policies have been considered in the optimization of the integrated energy system. One of the most effective policies is the subsidized price of electricity in Iran. The low cost of electricity, along with the high cost of initializing and maintaining integrated system equipment, has made the system tend to supply power from the grid when exergy efficiency and cost are considered objective functions. In this case, the system has purchased 501.9 MWh of electricity from the grid, which is the highest value among the scenarios. Accordingly, the tendency to use gas turbines has decreased. The lowest gas turbine capacity is allocated to this scenario, which is 10.45 kWh. The use of solar equipment for heating is faces cost constraints. Therefore, 17 rows of PVT and a solar collector with an area of 6.75 m^2 have been used in this scenario. The results show that only 119.4 MWh of the electricity and 486.14 MWh of the heat required by the system are supplied by solar energy. A small part of the heat is also provided by the heat recovery boiler. Most of the heat demand is generated by the auxiliary boiler. This value is 677.7 MWh, which is more than other scenarios. The heat stored in the tank is 145.7 MWh, which is related to the second optimization pattern. Heat production by upstream equipment such as the gas turbine, solar collector, and PVT panels is not significant, so most of the heat shortage is provided by the auxiliary boiler.

There are some limitations and advantages to using all parameters of exergy efficiency, cost rate, and pollution index as the objective functions of optimization. But except in special cases, all objective functions are very important. Choosing an optimal system with the highest efficiency, least pollution, and lowest cost is the main priority in designing an integrated energy system for a building. Accordingly, three-objective optimization will suggest the best performance of the energy system. The optimization results show that the system has used solar equipment properly in this case. The use of 20 rows of PVT and a solar collector with an area of 5.27 m^2 has provided 144.1 MWh of the electricity demanded by the sun. Also, 583.06 MWh of the heat required by the building and the chiller generator is absorbed by the solar subsystems (Fig. 20). In addition, Fig. 20 shows that solar power generation depends on the amount of heat received per hour. The results show that the maximum heat and electricity from the solar systems are 341.9 kWh and 84.37 kWh, respectively. In this case, 55.05 MWh electricity was also sold to the grid during the year. It is predictable that in the warmer seasons of the year when solar radiation is higher, the rate of heat absorption and solar power generation will also increase. Based on this, the highest average monthly heat and power absorption occurred in January and are equal to 97.3 kWh and 24 kWh, respectively. Also, the minimum values are related to December, which are 30.86 kWh and 7.66 kWh, respectively.

Positive values in Fig. 21 mean generating additional electricity and selling it to the grid. It is noteworthy that these values are related to the monthly average. Negative values mean a shortage of electricity generated by PVT and the gas turbine. In this case, the electricity shortage is compensated by purchasing from the network. The results of this figure show

that except for July and August, in other months the average monthly excess electricity is negative and the result is the purchase of electricity from the grid in these months. The highest amount of electricity sold to the grid occurred in July, with an average monthly amount of 14.4 kWh. The reason for the possibility of selling electricity these months can be seen in Fig. 2. These two months are related to the university holidays, as a result of which the electrical load of the building has decreased. Most electricity purchases from the grid were made in November. The average purchase of electricity this month is calculated at 29.4 kWh. The figure also shows that during the colder months of the year, when PVT power generation decreased, the amount of electricity purchased from the grid increased. Approximately 204.2 MWh of electricity was purchased from the grid during a year. The capacity of the gas turbine in this scenario is 37.43 kWh, and the whole PVT power generation during the year is 144.1 MWh. This equipment provides part of the electricity required by the system, but there is a greater tendency to buy electricity from the grid.

Figure 22 shows the amount of excess heat in the upstream subsystems. These points represent the difference between the total heat produced (solar collector, PVT, and heat recovery boiler) and the demanding heat. Positive values in this diagram mean the production of excess heat. The total annual heat stored in the tank is 2300 MWh. The results of this figure show that the highest excess heat was 113.4kWh, which occurred in March. The second average monthly excess of heat is related to November. The reason for this higher parameter in March is the lower need of the building for heat in these months, as well as the approach of spring and the acceptable increase in the average heat produced by the solar collector and PVT. Negative values are the amount of heat shortage that must be provided by the boiler, which is 288.4 MWh per year. The highest heat demand through the boiler is 58kWh (monthly average) in June. This month has the most cooling. This means that the absorption chiller generator will need a significant amount of heat this month. The corresponding amounts of heat supplied by the auxiliary boiler are shown in Fig. 23 for fuel consumption. The total fuel consumption of the boiler is 23.08 Ton/year in this case.

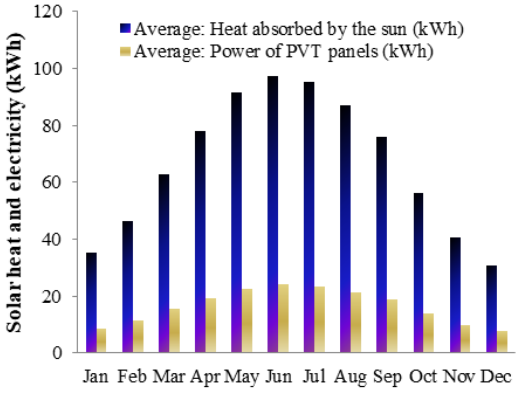

Fig. 20. Heat and electricity generated by solar subsystems (average per month)

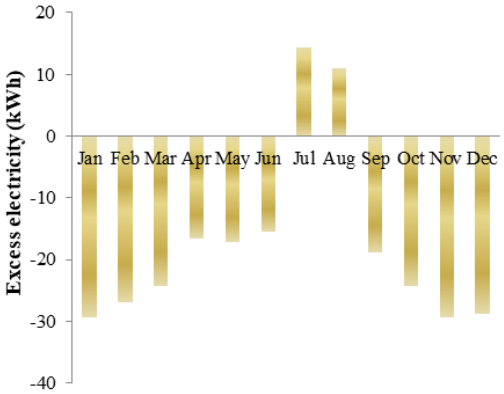

Fig. 21. The difference between power production by upstream subsystems (PVT and GT) and electricity demand (average per month)

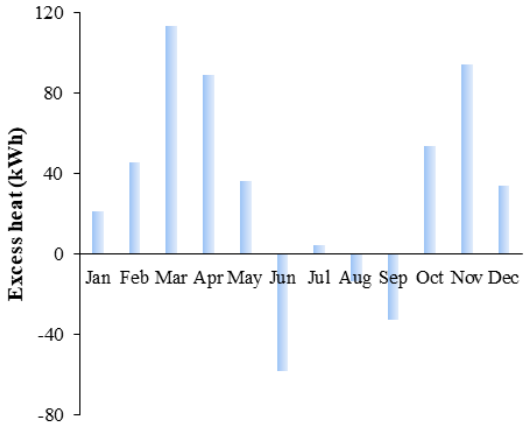

Fig. 22. The difference between heat production by upstream subsystems (PVT, solar collector and, HRB) and heat consumption (average per month)

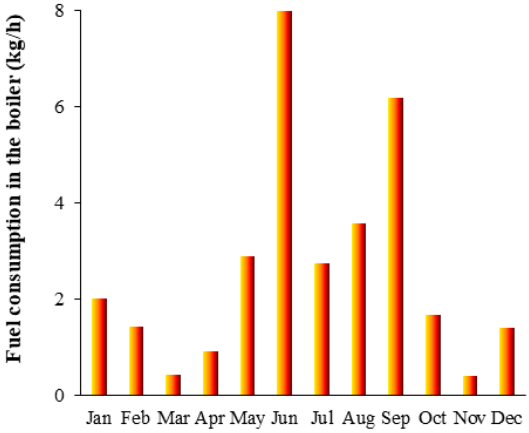

Fig. 23. Boiler fuel consumption (average per month)

5. Conclusion

We have presented the optimization results for an integrated fossil-solar energy system to provide the dynamic loads of a real model. The studied model is a six-story educational building located in Tehran. Two optimization methods have been used. In the two-objective optimization, the parameters of exergy efficiency, pollution index, and cost rate are considered in pairs as optimization functions. The three-objective optimization model selects all three parameters as objective functions. The results obtained from the optimization are as follows:

- Maximum usage of solar subsystems occurs when exergy efficiency and pollution are selected as objective functions of optimization. In this case, 68 rows of PVT and a solar collector with an area of 6.25m^2 have been used. As a result, the highest solar thermal and electric energy production are 1945.9 MWh and 484.5 MWh, respectively.
- Maximum electricity purchased from the grid is 501.9 MWh which occurs in a situation where the total cost rate and exergy efficiency are optimization objectives. The subsidized price of electricity is the reason for this result. Accordingly, the lowest capacity for a gas turbine (10.45 kWh) is obtained in this case.
- If the pollution index is ignored in optimization, the auxiliary boilers will be the main equipment for heat supply. The highest heat supplied by the boiler is 677.7 MWh in this case. However, the calculated pollution index is 767 g/kWh for such a situation.
- The highest efficiency loss occurs for the integrated system by considering cost rate and emission as the objective functions of optimization. Exergy efficiency has reached 37.88%. Also, the pollution index and total cost rate are 171 g/kWh and 2.1 $/h, respectively, which are lower than the corresponding values in other scenarios.
- Exergy efficiency at the best point of system performance in three-objective optimization is 50.21%. In this case, the tendency to buy electricity from the grid is greater than the in-sit production of electricity. The cost of production per kWh of electricity is 7.1 $, and the pollution index of CO_2 emission is 301 g/kWh.
- The system can sell the electricity to the grid in July and August, and the highest average monthly electricity sale is 14.4 kWh in July.
- The highest average monthly electricity purchase of 29.4 kWh occurs in November. Required electricity

purchases in other months are less than that in November.

- The highest heat is stored in March. The average monthly excess heat in this month is 113.4kWh.
- The highest output of the boiler takes place in January. The average heat supplied by the boiler this month is 58kWh.

References

[1] Nikbakht Naserabad S., Mobini K., Mehrpanahi A., Aligoodarz M.R., Exergy-energy analysis of full repowering of a steam power plant, Frontiers in Energy (2015) 9:54–67.

[2] Sajadi B., Mirnaghi M., Akhavan-Behabadi M.A., Delgarm N., Goudarzi A., Simulation-based optimization of smart windows performance using coupled EnergyPlus - NSGA-II - ANP method, Energy Equipment and Systems (2021) 9(1):1-13.

[3] Heydari A., Sadati S.E., Gharib M.R., Effects of different window configurations on energy consumption in building: Optimization and economic analysis, Journal of Building Engineering (2021) 35:102099.

[4] Chen B., Liu Q., Chen H., Wang L., Deng T., Zhang L., Wu X., Multiobjective optimization of building energy consumption based on BIM-DB and LSSVM-NSGA-II, Journal of Cleaner Production (2021) 294:126153.

[5] Ilbeigi M., Ghomeishi M., Dehghanbanadaki A., Prediction and optimization of energy consumption in an office building using artificial neural network and a genetic algorithm, Sustainable Cities and Society (2020) 61:102325.

[6] Feng J., Luo X., Gao M., Abbas A., Xu Y.P., Pouramini S., Minimization of energy consumption by building shape optimization using an improved Manta-Ray Foraging Optimization algorithm, Energy Reports, (2021) 7:1068-1078.

[7] Ebrahimi-Moghadam A., Ildarabadi P., Aliakbari K., Fadae F., Sensitivity analysis and multi-objective optimization of energy consumption and thermal comfort by using interior light shelves in residential buildings, Renewable Energy (2020) 159:736-755.

[8] Behzadi A, Arabkoohsar A., Yang Y., Optimization and dynamic techno-economic analysis of a novel PVT-based smart building energy system, Applied Thermal Engineering (2020) 181:115926.

[9] Braun R., Haag M., Stave J., Abdelnour N., Eicker U., System design and feasibility of trigeneration systems with hybrid photovoltaic-thermal (PVT) collectors for zero energy office buildings in different climates, Solar Energy (2020) 196:39-48.

[10] Herrando A., Pantaleo A.M., Wang K., Markides C.N., Solar combined cooling, heating and power systems based on hybrid PVT, PV or solar-thermal collectors for building applications, Renewable Energy (2019) 143:637-647.

[11] Mago P.J., Smith A.D., Evaluation of the potential emissions reductions from the use of CHP systems in different commercial buildings, Building and Environment (2012) 53:74-82.

[12] Barbieri E.S., Melino F., Morini M., Influence of the thermal energy storage on the profitability of micro-CHP systems for residential building applications, Applied Energy, (2012) 97:714-722.

[13] Celador A.C., Iribarren E.P., Sala J.M., del Portillo-Valdés L.A, Thermoeconomic analysis of a micro-CHP installation in a tertiary sector building through dynamic simulation, Energy (2012) 45:228-236.

[14] Smith A.D., Mago P.J., Fumo N, Benefits of thermal energy storage option combined with CHP system for different commercial building types, Sustainable Energy Technologies and Assessments (2013) 1:3-12.

[15] Knizley A., and Mago P.J, Evaluation of combined heat and power (CHP) systems performance with dual power generation units for different building configurations, International Journal of Energy Research (2013) 37:1529–1538.

[16] Pirkandi J., Jokar M.A., Sameti M., Kasaeian A., Kasaeian F., Simulation and multi-objective optimization of a combined heat and power (CHP) system integrated

with low-energy buildings, Journal of Building Engineering (2016) 5:13-23.

[17] Kayoa G., Hasanb A., Siren K., Energy sharing and matching in different combinations of buildings, CHP capacities and operation strategy, Energy and Buildings (2014) 82:685-695.

[18] Adam A., Fraga E.S., Brett D.J.L., Options for residential building services design using fuel cell based micro-CHP and the potential for heat integration, Applied Energy (2015) 138:685-694.

[19] Liu N., Wang J., Yu X., Ma L., Hybrid Energy Sharing for Smart Building Cluster With CHP System and PV Prosumers: A Coalitional Game Approach, IEEE Access (2018) 6:34098–34108.

[20] Amber K.P., Dunn A., Parkin J., Day A.R., Development of a Combined Heat and Power Sizing Model for Higher Education Buildings in the United Kingdom, Energy and Buildings (2018) 172:537-553.

[21] Lei H., Dongjiang H., Jinfu Y., Changliang T., Long H., Study on different heat supplementation strategies for a combined cooling, heating and power system, Applied Thermal Engineering (2018) 144:558-579.

[22] Ashouri M., Razi Astaraei F., Ghasempour R., Ahmadi M.H., Feidt M., Optimum insulation thickness determination of a building wall using exergetic life cycle assessment, Applied Thermal Engineering (2016) 106:307-315.

[23] Hanafizadeh P., Eshraghi J., Ahmadi P., Sattari A, Evaluation and sizing of a CCHP system for a commercial and office buildings, Journal of Building Engineering (2016) 5:67-78.

[24] Lu Y., Wang S., Zhao Y., Yan C., Renewable energy system optimization of low/zero energy buildings using single-objective and multi-objective optimization methods, Energy and Buildings (2015) 89:61-75.

[25] Capstone Turbine Corporation, Capston C200 Technical Documents - 410066 Rev C, 2009.

[26] Incropera F.P., Fundamentals of Heat and Mass Transfer (2011) John Wiley & Sons.

[27] Ondeck A., Edgar T.F., Baldea M., A multi-scale framework for simultaneous optimization of the design and operating strategy of residential CHP systems, Apply Energy (2017) 205:1495–1511.

[28] Rovira A., Valdés M., Durán M.D., A model to predict the behaviour at part load operation of once-through heat recovery steam generators working with water at supercritical pressure, Apply Thermal Engineering (2010) 30:1652–1658.

[29] Ganapathy V., Heat recovery steam generators: performance management and improvement, Power Plant Life Management and Performance Improvement, Woodhead Publishing Series in Energy (2011) PP. 606-634. doi:10.1533/9780857093806.5.606.

[30] Dinçer I., Rosen M.A., Ahmadi P., Optimization of Energy Systems, Wiley, 2017.

[31] Herold K.E., Radermacher R., Klein S.A., Absorption Chillers and Heat Pumps, (2016) 2nd Edition.

[32] ENERGY PLUS, Engineering Reference, (2015).

[33] Gershon Grossman J.E.R., Absorption Systems for Combined Heat and Power: The Problem of Part-Load Operation, ASHRAE Trans. 109 (2003).

[34] DiOrio N., Christensen C., Burch J.M., Dobos A., Technical Manual for the SAM Solar Water Heating Model, NREL, March 31, 2014. Online: https://sam.nrel.gov/images/web_page_files/diorio-2014-draft-swh-sam-technical-manual.pdf.

[35] Guarracino I., Mellor A., Ekins-Daukes N.J., Markides C.N., Dynamic coupled thermal-and-electrical modelling of sheet-and-tube hybrid photovoltaic/thermal (PVT) collectors, Applied Thermal Engineering (2016) 101:778-795.

[36] Maghsoudi Mehrabani K., Mehrpanahi A., Rouhani V., Nikbakht Naserabad S., Study of the effect of using duct burner on the functional parameters of the two repowered cycles through exergy analysis, Thermal Science (2017) 21(6-B):3011-3023.

[37] Maghsoudi Mehrabani K., Mehrpanahi A., Rouhani V., Nikbakht Naserabad S.,

Using two types of heat recovery steam generator for full repowering a steam power plant and its analysis by exergy method, Indian Journal of Scientific Research (2014) 1(2):106-119.

[38] Maghsoudi Mehrabani K., Mehrpanahi A., Fani Yazdi S.S., Nikbakht Naserabad S., Optimization of Exergy in Repowering Steam Power Plant by Feed Water Heating Using Genetic Algorithm, Indian Journal of Scientific Research (2014) 1(2):183-198.

[39] Mehrpanahi A., Nikbakht Naserabad S., Ahmadi G., Multi-objective linear regression based optimization of full repowering a single pressure steam power plant, Energy (2019) 179:1017-1035.

[40] Hanafizadeh P., Mirzakhani Siahkalroudi M., Akhavan Bahabadi M.A., Investigation of a single-reheat condensing steam power plant based on energy and exergy analysis, Energy Equipment and Systems (2014) 2(2):155-170.

[41] Nikbakht Naserabad S., Mobini K., Mehrpanahi A., Aligoodarz M.R., Multi Objective Optimization of Converting an Old Steam Power Plant to Combined Cycle Power Plant (CCPP) using Double and Single Pressure Heat Recovery Steam Generator (HRSG) via Genetic Algorithm, Journal of Applied and Computational Sciences in Mechanics (2016) 27(2):129–139.

[42] Nikbakht Naserabad S., Mehrpanahi A., Ahmadi G., Multi-objective optimization of HRSG configurations on the steam power plant repowering specifications, Energy (2018) 159:277-293.

[43] Nikbakht Naserabad S., Mobini K., Mehrpanahi A., Aligoodarz M.R., Exergy-energy analysis of full repowering of a steam power plant, Frontiers in Energy (2015) 9:54–67.

[44] Nikbakht Naserabad S., Mobini K., Mehrpanahi A., Aligoodarz M.R., Technical Analysis of Conversion of A Steam Power Plant to Combined Cycle, Using Two Types of Heavy Duty Gas Turbines, International Journal of Engineering TRANSACTIONS B: Applications (2015) 28(5):781-793.

[45] Mostafavi Sani M., Noorpoor A., Shafie-Pour Motlagh M., Design and optimization of an energy hub based on combined cycle power plant to improve economic and exergy objectives, Energy Equipment and Systems (2020) 8(1):1-22.

[46] Wang J., Chen Y., Lior N., Li W., Energy, exergy and environmental analysis of a hybrid combined cooling heating and power system integrated with compound parabolic concentrated-photovoltaic thermal solar collectors, Energy (2019) 185:463-476.

[47] Nikbakht Naserabad S., Rafee R., Saedodin S., Ahmadi P., A novel approach of tri-objective optimization for a building energy system with thermal energy storage to determine the optimum size of energy suppliers, Sustainable Energy Technologies and Assessments (2021) 47:101379.

[48] Fakhari I., a, Peikani P., Moradi M., Ahmadi P., An investigation of optimal values in single and multi-criteria optimizations of a solar boosted innovative tri-generation energy system, Journal of Cleaner Production (2021) 316:128317.

[49] Nikbakht Naserabad S., Mehrpanahi A., Ahmadi G., Multi-objective optimization of feed-water heater arrangement options in a steam power plant repowering, Journal of Cleaner Production (2019) 220:253-270.

[50] Nikbakht Naserabad S., Rafee R., Saedodin S., Ahmadi P., Multi-objective optimization of a building integrated energy system and assessing the effectiveness of supportive energy policies in Iran, Sustainable Energy Technologies and Assessments (2021) 46:101343.

[51] Nabati A.M., Sadeghi M.S., Nikbakht Naserabad S., Mokhtari H., Izadpanah S., Thermo-economic analysis for determination of optimized connection between solar field and combined cycle power plant, Energy (2018) 162:1062-1076.